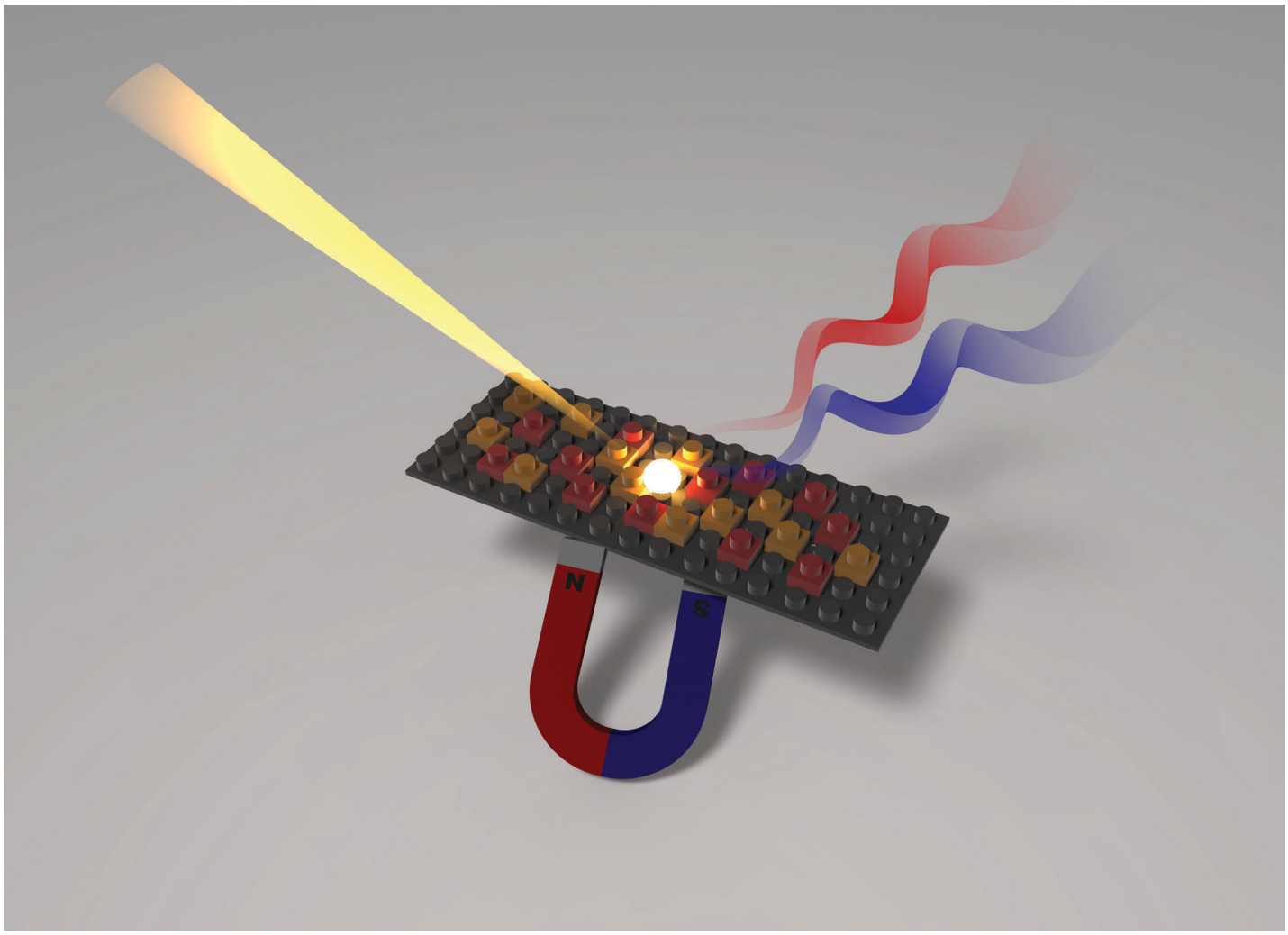

Showcasing research from the group of Professor Jaebeom Lee at the Department of Cogno-Mechatronics Engineering, Pusan National University, Republic of Korea and Dr Jaewook Lee at the RIGST, Shizuoka University, Japan.

Magneto-optically active magnetoplasmonic graphene

Magnetoplasmonic graphene (PMGRP) decorated with Au NPs and MNPs showed excellent magneto optical activity. And this two-dimensional nanocomposite with magnetic and optical property can contribute to various fields such as memory or optoelectronic devices, sensing platforms, energy harvesting, and biomedical MO devices.

As featured in:

See Jaewook Lee and Jaebeom Lee, *Chem. Commun.*, 2017, **53**, 5814.

ROYAL SOCIETY OF CHEMISTRY

rsc.li/chemcomm

Registered charity number: 207890

ChemComm

COMMUNICATION

View Article Online
View Journal | View Issue

Cite this: *Chem. Commun.*, 2017, 53, 5814

Received 15th February 2017,
Accepted 9th April 2017

DOI: 10.1039/c7cc01207a

rsc.li/chemcomm

Magneto-optically active magnetoplasmonic graphene†

Jaewook Lee [ab] and Jaebeom Lee *[a]

Two-dimensional nanocomposites with magnetic and optical properties were investigated for novel magneto-optical (MO) applications. Such an MO effect could be induced and enhanced by synergistic properties with magnetic and plasmonic coupling. In this study, magnetoplasmonic graphene (MPGRP) decorated with Au nanoparticles (NPs) and magnetic NPs (MNPs) was simply prepared as a 2D MO active material. This MPGRP exhibited superparamagnetic behaviour at room temperature and strong MO activity, resulting from magnetic spin from the MNPs and electron spin from the Au NPs on one graphene sheet, which is beneficial for memory or optoelectronic devices, sensing platforms, energy harvesting, and biomedical MO devices.

Synergistic characteristics of assembled nanostructures such as plasmonic coupling, surface-enhanced Raman scattering (SERS), and magneto-optical (MO) properties have attracted attention.[1–3] Nanocomposites with two-dimensional (2D) magnetic and optical properties are particularly unique because their electron- and spin-oriented structure can induce light polarization *via* the MO effect under a magnetic field. The phenomenon of light polarization could be induced by structural orientation of plasmonic or fluorescent materials such as chiral-oriented Au nanorods,[4,5] assembly of plasmonic nanoparticles (NPs)/chiral materials,[6] chiral graphene QDs[7] and so on. On the other hand, in order to improve such an interesting and useful optical phenomenon, the magnetoplasmonic effect has been introduced,[8] and several MO materials have been investigated including graphene (GRP) based 2D structure, magnetic/plasmonic hybrid materials and so on.[9–11] In particular, GRP could contribute a small portion of the magnetoplasmonic effect due to its plasmonic excitation.[11] Thus, GRP could tune the MO effect eventually *via* Faraday rotation, even if it does not have magnetic properties.[12] Indeed, such MO-active materials can be applied for various applications, not only for light polarizers but also for memory storage devices, magnetic field sensors, and non-linear optical devices.[13–16] Thus, many researchers have desired to develop new hybrid 2D structures that possess MO activity,[15–17] and NP-decorated GRP has been regarded as a potential candidate. However, the decoration process is complex and requires harsh chemical and physical processes such that generally, a single type of NP-decorated GRP has been developed using a metal or metal oxide.[18–21] In our study, a magnetoplasmonic graphene (MPGRP) sheet was successfully produced with both Au NPs and magnetic NPs (MNPs) at room temperature *via* a simultaneous exfoliation and reduction mechanism, *i.e.*, both Au NPs and MNPs were bound onto the graphene surface, where oxidizable gallic-acid-modified MNPs (GA-MNPs) were used as a reducing agent.[22] The two-step reaction of the MPGRP synthesis process is illustrated in Fig. 1: (I) π electrons induce binding of Au^{3+} ions onto the graphene surface during sonication, and (II) the Au ions are subsequently converted into Au NPs on the graphene surface *via* oxidizable GA-MNPs, which serve as a mild reducing agent. At the same time, the benzene rings on GA-MNP lead to a π–π interaction between the graphene surface and MNPs. Finally, binary NP-decorated graphene with Au NPs and MNPs can be produced. The detailed synthesis process of MPGRP is described in the ESI.† The GA-MNPs exhibit an average diameter of 12 nm (Fig. S1, ESI†); the carboxylic part of GA is attached to the MNP surface, and the three unbound hydroxyl groups of GA prevent the agglomeration of the GA-MNPs and reduce the Au^{3+} ions into Au-NPs.

Fig. 2a and b present the electron microscopy images of the MNPs and Au NP-decorated graphene. All the particles are widely dispersed on the graphene surface. Because the electron density on the surface of the Au NPs is higher than that of the MNPs, the Au-NPs appear to be darker than the MNPs in the transmission electron microscopy (TEM) images, and the graphene layer appears to be transparent. In the scanning electron microscopy (SEM) images of the graphene flakes and MPGRP, a clean surface of graphene is observed before the reaction, whereas a large number of NPs are found on both surfaces of the exfoliated graphene layers (Fig. 2c). In the SEM image, two different NPs (red and brown arrows) are also observed, which

[a] *Department of Cogno-Mechanical Engineering, Pusan National University, Busan 609-735, Republic of Korea. E-mail: jaebeom@pusan.ac.kr*
[b] *Research Institute of Green Science and Technology, Shizuoka University, Shizuoka, 422-8529, Japan*

† Electronic supplementary information (ESI) available. See DOI: 10.1039/c7cc01207a

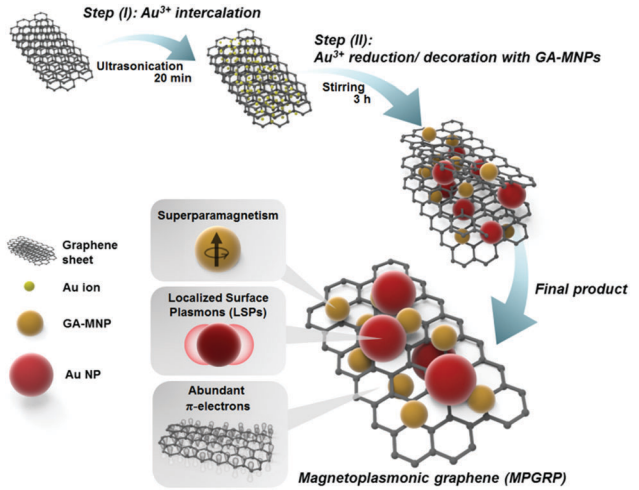

Fig. 1 Schematic illustration of MPGRP preparation *via* a two-step approach.

corresponds well to the TEM images. In addition, the plasmonic properties of the MPGRP were monitored using UV-vis spectroscopy and Raman spectroscopy. Typically, the plasmonic peak of Au NPs is clearly observed at approximately 525 nm; however, in this case, a broad absorption band appears at approximately 510–650 nm (Fig. 2d). In addition, this spectrum appears to exhibit tailing behaviour. It is assumed that the main resonance spectrum may have merged with a second plasmonic band in the MPGRP hybrid structure. Generally, the presence of a second band is associated with plasmonic interactions among the noble metallic NPs, *e.g.*, in the longitudinal direction of one-dimensional nanostructures.[19,20,23] Because graphene possesses π electrons, plasmonic coupling can occur between two Au NPs. This means that an interaction between π electrons on the GRP structure and the plasmon based electron cloud of an individual Au NP could occur by orbital overlap, and as a result, plasmonic coupling between closely located Au NPs could be occurred through π electrons on GRP.[24,25] In addition, the solution turned purple when iron was combined with GA, thus implying that this absorption band was merged with the Au plasmonic band. Therefore, the absorption band of the MPGRP was wide and broad. Fig. 2e presents the Raman spectra of graphene and MPGRP at an excitation wavelength of 514 nm. In both spectra, a D peak at 1340 cm^{-1} and a G peak at approximately 1580 cm^{-1} were observed. The intensity of the spectrum of the MPGRP (red line) was four times greater than that of the graphene flakes (black line). It is probable that this SERS effect was induced by the Au NPs on the graphene surface.[24,25] The magnetization of the MPGRP was measured using a superconducting quantum interference device (SQUID) at room temperature (300 K) and under liquid He (4.2 K) between −30 kOe and 30 kOe. Under both conditions, the M–H relationship consisted of a non-linear and reversible hysteresis loop. In Fig. 2f, when the applied magnetic field is zero, the remanence effect is 1.06 emu g^{-1} at 300 K. In this case, the coercive force of the MPGRP was measured to be approximately 17.8 Oe. At 4.2 K (in Fig. S2, ESI†), there was an approximately ten-fold increase in the remanence effect (10.5 emu g^{-1}); the coercive force also exhibited the same tendency (198.3 Oe). Therefore, the dual-decorated nanocomposite in this study clearly exhibited superparamagnetic behaviour. In addition, MPGPR movement was also observed depending on the magnetic field. In Fig. 1f (inserted image), the MPGRP is dispersed in deionized (D.I.) water without a magnetic bar; however, when the magnetic bar is near the

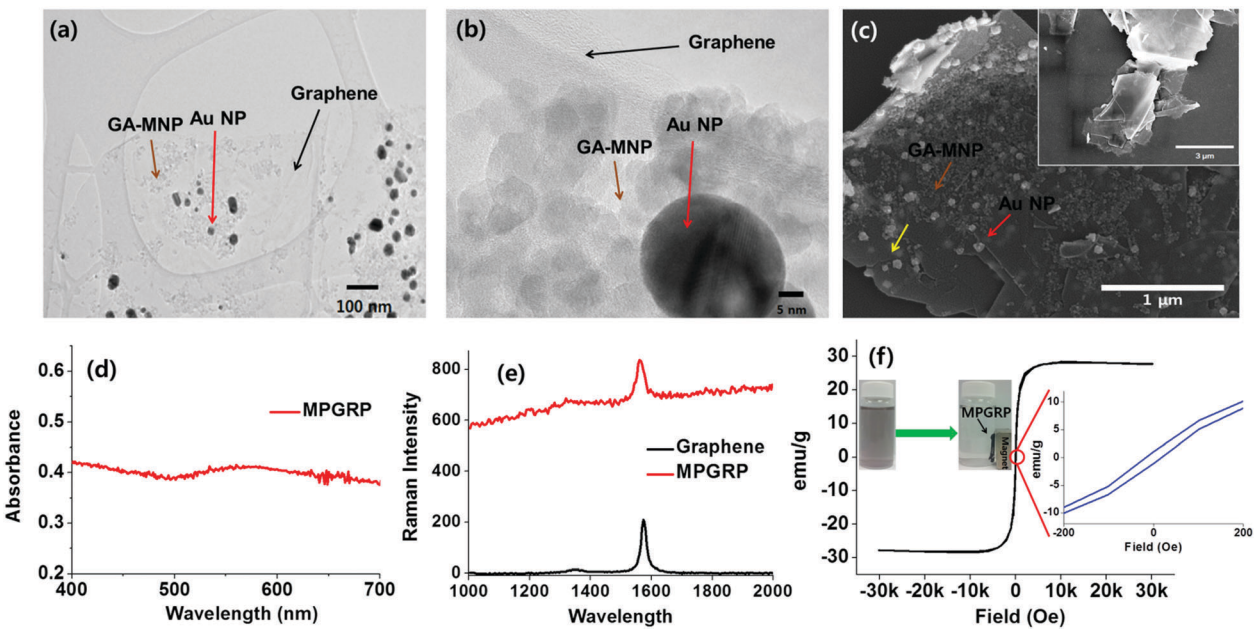

Fig. 2 TEM images of the MPGRP at (a) low magnification (×15k) and (b) high magnification (×300k), (c) SEM image of the MPGRP, where the red and brown arrows represent the Au-NP and MNP, respectively, and the yellow arrow represents NPs located on the opposite face of graphene (inset: pristine graphene flake). (d and e) UV-vis and Raman spectra of MPGRP. (f) SQUID hysteresis loops of MPGRP at 300 K (inset: photographs showing the movement of MPGRP in the absence/presence of a magnet).

nanocomposite, the MPGRP is attracted to the magnet because of its superparamagnetism. The MO properties of the newly synthesized MPGRPs were then carefully characterized. The magneto-optical activity of the MPGPR was evaluated using magnetic circular dichroism (MCD) measurements (Fig. 3a). First, the GA-MNPs and MPGRP were dispersed in D.I. water, and MCD was subsequently measured (Fig. 3b and c). The GA-MNPs did not exhibit chirality without a magnetic field (Fig. 3b, blue spectrum). However, under an applied magnetic field of 1.4 T, polarity occurred where three major MO transitions took place: $[Fe^{2+}]t_{2g} \rightarrow (Fe^{3+})t_2$, at approximately 485 nm; $(Fe^{2+})t_2\ [Fe^{3+}]e_g$, at approximately 350 nm; and $[Fe^{2+}]e_{2g} \rightarrow (Fe^{3+})t_2$, at approximately 305 nm, which originated from the MNP.[26–28]

The MCD signal changes depending on the direction of the magnetic field (NS and SN); however, the spectra are clearly symmetric.[29] The intensities of the spectra are also similar. Free spins in the ferrous sites of Fe_3O_4 magnetic particles are known to induce a magnetic moment.[30] Thus, these spins are moved up and down by an external magnetic force. In Fig. 3b, the two green arrows at 241 and 456 nm indicate that the spin rotation is zero because the polarity is 0 mdeg.[2] Specifically, magnetically polarized spins (through the external magnetic field) do not interact with the incident light of these wavelengths. Regardless of the magnetic field direction (NS ↔ SN), the zero points of the rotation of the polarized spins are identical. The MPGRP MCD spectra are similar to those of the GA-MNP case, and the behaviour of its transitions was measured, as shown in Fig. 3c. However, the zero points of the rotation of the polarized spins vary depending on the direction of the applied magnetic fields. In detail, the cross points (green arrows in Fig. 3c) of the two spectra are not at 0 mdeg but at −2 and 0.5 mdeg, respectively, and the wavelengths also shift from 241 nm (for GA-MNP) to 245 nm (for MPGRP) and from 457 nm (for GA-MNP) to 465 nm (for MPGRP) due to the localized surface plasmons on the MPGRP structure.[31] Furthermore, the absolute value of the intensity varies depending on the magnetic field direction. When the magnetic field is in the N/S direction, the highest intensity is approximately 29 mdeg, whereas in the S/N direction, the highest intensity is −35 mdeg. In general, the MO transition of the Au-NPs is observed near the plasmonic absorption wavelength range even though the MO contribution of the Au NPs is not clearly observed for the solution used in this study (Fig. 3c).[32,33] On the other hand, graphene does not possess magnetic properties. Thus, its MCD spectra signal is not as strong as that of a magnetic nanoparticle (Fig. S3a, ESI†). Nevertheless, depending on the magnetic field direction (N/S, N/S), the MCD spectra of graphene showed different behaviour around 300 nm (blue arrow). Eventually, according to the UV/vis spectrum of graphene (Fig. S3b, ESI†), electron transition (energy level transition) of graphene could be monitored around 300 nm (green arrow). This means that electrons in this region might interact with the external magnetic field and as a result, a weak MCD signal of graphene could be measured depending on the magnetic field. On the other hand, the MPGRP could freely move in D.I. water *via* an external magnetic force. Thus, the observation of the solution-based MCD may not be accurate. Thus, to prevent this type of behaviour, the MO activity of the MPGRP was measured in its film form. To prepare the transparent film, the GA-MNP or MPGRP was mixed with polyacrylic acid (PAA) and subsequently solidified. The GA-MNP film exhibited MCD spectra similar to the solution spectra (Fig. 3d). However, the MPGRP film produced a completely different spectrum from that of the solution. For example, the MO activity did not behave in an opposite manner when the direction of the magnetic field was changed (Fig. 3e), and an abnormal spin movement was exhibited. In the film, the MO contribution of the Au-NPs was clearly observed, and the MCD spectra correlated with the UV-vis spectrum of the MPGRP (Fig. 3e, blue arrow). Furthermore, the MO effect of the MPGRP was obviously exhibited. Thus, it is clear that the spins of the MNPs strongly interacted with the plasmon resonance of graphene and Au NPs.

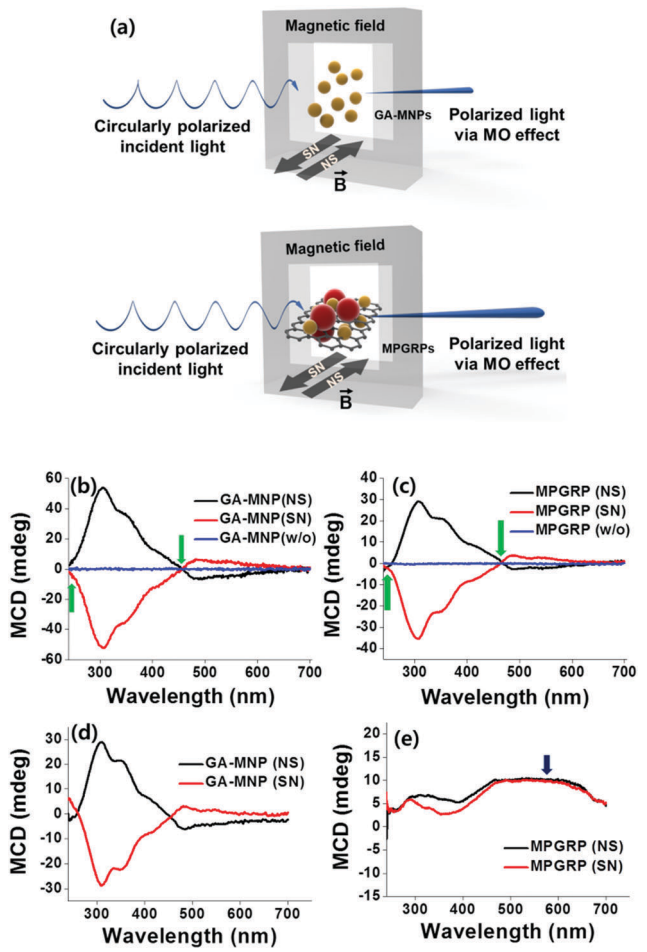

Fig. 3 (a) Illustration of MO activity measurement, (b) MCD spectra of GA-MNP and (c) MPGRP in D.I. water as a solution phase, (d) MCD spectra of GA-MNP and (e) MPGRP in PAA films under an applied magnetic field of 1.4 T.

Fig. 4a and b present the sum value of the NS- and SN-polarized spin rotation angles from the response of MCD. The intensity of the MPGRP spectrum is greater than that of the GA-MNP spectrum because of its electromagnetic field. This phenomenon can be explained by the MO effect and Faraday rotation (FR). The MO effect occurs through the interaction between electromagnetic waves and the medium in a magnetic

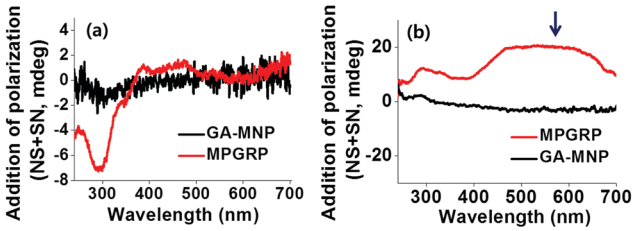

Fig. 4 (a) Solution cases (free motion is available) and (b) PAA film cases (a rigid environment) under an applied magnetic field of 1.4 T.

field. In addition, this MO effect can be enhanced by a composite containing both a plasmonic material and a magnetic material. The FR of the material varies in left-polarized and right-polarized light around the magnetic field. As previously mentioned, the MPGRP possesses both magnetic and plasmonic properties; *i.e.*, the MNPs possess free electrons that produce the magnetic properties at the d-orbital of the ferric site, whereas graphene and Au NPs possess plasmonic properties. In particular, the greatest difference (indicated by the arrow in Fig. 4b) between the spectra obtained under differently polarized light was located at a similar wavelength to that of the plasmonic absorption of the Au-NPs. Both the plasmonic and magnetic factors can interact with the incident light in the magnetic field, which produces the difference in the light polarizability observed in this system. Therefore, it can be concluded that the MPGRP is an MO-active material.

In conclusion, MO-active MPGRP was successfully synthesized *via* a GA-MNP-assisted synthesis route without any thermal assistance or the use of harsh reducing agents. The MO effect of the MPGRP was observed by MCD measurements. In a magnetic field, the MPGRP induces light polarization. Consequently, the MPGRP possesses a unique MO effect and has excellent prospects for use in applications such as memory devices, sensors, displays, optoelectronic devices, energy-harvesting devices, MRI equipment, and hyperthermia applications.

The authors thank Dr Nicholas A. Kotov for allowing them to use the MCD spectroscope, and they are grateful for his excellent advice on MO effect research. This study was supported by a grant from the Korean Health Technology R&D Project of the Ministry of Health & Welfare, Republic of Korea (A110191, HI16C1553), and the National Research Foundation of Korea (NRF) grant funded by the Korean government (MEST) (NRF-2016R1A2B4012072)

Notes and references

1 X. Q. Fu, F. L. Bei, X. Wang, S. O'Brien and J. R. Lombardi, *Nanoscale*, 2010, **2**, 1461–1466.
2 P. K. Jain, Y. H. Xiao, R. Walsworth and A. E. Cohen, *Nano Lett.*, 2009, **9**, 1644–1650.
3 A. Klinkova, R. M. Choueiri and E. Kumacheva, *Chem. Soc. Rev.*, 2014, **43**, 3976–3991.
4 B. Han, Z. Zhu, Z. Li, W. Zhang and Z. Tang, *J. Am. Chem. Soc.*, 2014, **136**, 16104–16107.
5 Z. Li, Z. Zhu, W. Liu, Y. Zhou, B. Han, Y. Gao and Z. Tang, *J. Am. Chem. Soc.*, 2012, **134**, 3322–3325.
6 W. Liu, Z. Zhu, K. Deng, Z. Li, Y. Zhou, H. Qiu, Y. Gao, S. Che and Z. Tang, *J. Am. Chem. Soc.*, 2013, **135**, 9659–9664.
7 N. Suzuki, Y. Wang, P. Elvati, Z. Qu, K. Kim, S. Jiang, E. Baumeister, J. Lee, B. Yeom, J. H. Bahng, J. Lee, A. Violi and N. A Kotov, *ACS Nano*, 2016, **10**, 1744–1755.
8 D. Bossini, V. I. Belotelov, A. K. Zvezdin, A. N. Kalish and A. V. Kimel, *ACS Photonics*, 2016, **3**, 1385–1400.
9 M. Autore, H. Engelkamp, F. D'Apuzzo, A. Di Gaspare, P. Di Pietro, I. Lo Vecchio, M. Brahlek, N. Koirala, S. Oh and S. Lupi, *ACS Photonics*, 2015, **2**, 1231–1235.
10 O. Boulle, J. Vogel, H. X. Yang, S. Pizzini, D. D. Chaves, A. Locatelli, T. O. Mentes, A. Sala, L. D. Buda-Prejbeanu and O. Klein, *Nat. Nanotechnol.*, 2016, **11**, 449–454.
11 I. Crassee, M. Orlita, M. Potemski, A. L. Walter, M. Ostler, Th. Seyller, I. Gaponenko, J. Chen and A. B. Kuzmenko, *Nano Lett.*, 2012, **12**, 2470–2474.
12 A. Politano and G. Chiarello, *Nanoscale*, 2014, **6**, 10927–10940.
13 M. Kataja, T. K. Hakala, A. Julku, M. J. Huttunen, S. van Dijken and P. Torma, *Nat. Commun.*, 2015, **6**, 7072.
14 M. Osada, N. Hajdukova-Smidova, K. Akatsuka, S. Yoguchi and T. Sasaki, *J. Mater. Chem. C*, 2013, **1**, 2520–2524.
15 M. Osada, Y. Ebina, K. Takada and T. Sasaki, *Adv. Mater.*, 2006, **18**, 295–299.
16 M. Osada, M. Itose, Y. Ebina, K. Ono, S. Ueda, K. Kobayashi and T. Sasaki, *Appl. Phys. Lett.*, 2008, **92**, 253110.
17 C. T. Ellis, A. V. Stier, M. H. Kim, J. G. Tischler, E. R. Glaser, R. L. Myers-Ward, J. L. Tedesco, C. R. Eddy, D. K. Gaskill and J. Cerne, *Sci. Rep.*, 2013, **3**, 3143.
18 M. Yang, B. G. Choi, T. J. Park, N. S. Heo, W. H. Hong and S. Y. Lee, *Nanoscale*, 2011, **3**, 2950–2956.
19 J. J. Liang, Y. Huang, J. Y. Oh, M. Kozlov, D. Sui, S. L. Fang, R. H. Baughman, Y. F. Ma and Y. S. Chen, *Adv. Funct. Mater.*, 2011, **21**, 3778–3784.
20 J. W. Qin, M. H. Cao, N. Li and C. W. Hu, *J. Mater. Chem.*, 2011, **21**, 17167–17174.
21 R. B. Rakhi, W. Chen, D. K. Cha and H. N. Alshareef, *J. Mater. Chem.*, 2011, **21**, 16197–16204.
22 J. Lee, S. Mulmi, V. Thangadurai and S. Park, *ACS Appl. Mater. Interfaces*, 2015, **7**, 15506–15513.
23 J. Lee, H. Zhou and J. Lee, *J. Mater. Chem.*, 2011, **21**, 16935–16942.
24 J. Lee, S. R. Ahmed, S. Oh, J. Kim, T. Suzuki, K. Parmar, S. S. Park, J. Lee and E. Y. Park, *Biosens. Bioelectron.*, 2015, **64**, 311–317.
25 J. Lee, J. Kim, S. R. Ahmed, H. Zhou, J. M. Kim and J. Lee, *ACS Appl. Mater. Interfaces*, 2014, **6**, 21380–21388.
26 P. J. vander Zaag, W. F. J. Fontijn, P. Gaspard, R. M. Wolf, V. A. M. Brabers, R. J. M. vandeVeerdonk and P. A. A. vanderHeijden, *J. Appl. Phys.*, 1996, **79**, 5936–5938.
27 K. J. Kim, H. S. Lee, M. H. Lee and S. H. Lee, *J. Appl. Phys.*, 2002, **91**, 9974–9977.
28 W. F. J. Fontijn, P. J. vander Zaag, M. A. C. Devillers, V. A. M. Brabers and R. Metselaar, *Phys. Rev. B: Condens. Matter Mater. Phys.*, 1997, **56**, 5432–5442.
29 H. Yao and Y. Ishikawa, *J. Phys. Chem. C*, 2015, **119**, 13224–13230.
30 Y. Ding, D. Haskel, S. G. Ovchinnikov, Y. C. Tseng, Y. S. Orlov, J. C. Lang and H. K. Mao, *Phys. Rev. Lett.*, 2008, **100**, 045508.
31 G. Armelles, A. Cebollada, A. Garcia-Martin and M. U. Gonzalez, *Adv. Opt. Mater.*, 2013, **1**, 10–35.
32 M. A. Zaitoun, W. R. Mason and C. T. Lin, *J. Phys. Chem. B*, 2001, **105**, 6780–6784.
33 F. Pineider, G. Campo, V. Bonanni, C. J. Fernandez, G. Mattei, A. Caneschi, D. Gatteschi and C. Sangregorio, *Nano Lett.*, 2013, **13**, 4785–4789.